Journal of
Microscopy

Journal of Microscopy, Vol. 245, Pt 2 2012, pp. 129–139
Received 23 February 2011; accepted 22 August 2011

doi: 10.1111/j.1365-2818.2011.03553.x

Analytical electron microscopy of black carbon and microaggregated mineral matter in Amazonian dark Earth

C.H. CHIA*, P. MUNROE*, S.D. JOSEPH*, Y. LIN*,
J. LEHMANN†, D.A. MULLER‡, H.L. XIN§ & E. NEVES¶
*School of Material Science and Engineering, University of NSW, Sydney, New South Wales, Australia
†Department of Crop and Soil Sciences, Cornell University, Ithaca, New York, USA
‡School of Applied and Engineering Physics, Cornell University, Ithaca, New York, USA
§Department of Physics, Cornell University, Ithaca, New York, USA
¶Instituto Nacional de Pesquisa da Amazonia, Manaus, Amazonas, Brazil

Key words. Black carbon, dark earths, EELS.

Summary

Black carbon (BC) is one of the most stable forms of soil organic matter. Its surface functional groups and structure have been well characterized by a range of analytical methods. However, little is known about the mechanisms of interactions between the BC particles and the surrounding mineral matter. In this paper a range of microscopy techniques, such as transmission electron microscopy and scanning transmission electron microscopy, were used to investigate the possible reactions of BC particles within microaggregates (<2 mm) found in Amazonian dark Earth. Attention is given to the interactions that occur at the interfacial regions between the organic and inorganic phases. Examination of Amazonian dark Earth showed that the carbon-rich phase detected within the BC particles has a significant calcium concentration and a high density of micropores was found at the BC–mineral interface. These observations provide evidence to support suggested mechanisms of interaction between these phases.

Introduction

Microaggregates formed via organic matter and mineral interactions are considered to be the repository of the most stable carbon pool in soils. Similarly, the largest proportion of carbon input into stable soil organic matter pools was found in microaggregates (Six *et al.*, 1998, 2001; Lehmann *et al.*, 2007). One of the supposedly most stable forms of soil organic matter is black carbon (BC), also being the oldest type of C found in soil (Schmidt & Noack, 2000). Although BC has been found within microaggregates (Glaser *et al.*, 2000; Brodowski *et al.*, 2005; Lehmann *et al.*, 2008), it is not clear to what extent BC particles interact with mineral matter (Nguyen *et al.*, 2008). The surfaces of BC particles found in Amazonian dark Earth (ADE) are enriched in elements such as P, Mg, Ca, Fe, Mg, Ti and Mn. ADEs also exhibit higher water holding capacity than the surrounding soil, higher pH and higher cation exchange capacity. These properties act to sustain greater fertility compared to the intensely weathered acidic adjacent soils that are poor in BC (Liang *et al.*, 2006).

The external and internal structure of ADE has been examined using a range of analytical techniques including nuclear magnetic resonance (Novotny *et al.*, 2006; Novotny *et al.*, 2007; Novotny *et al.*, 2009), Fourier transform infrared spectroscopy, C (1s) near edge X-ray absorption fine structure (NEXAFS) spectroscopy (Solomon *et al.*, 2007), scanning electron microscopy (SEM; Glaser *et al.*, 2000; Lima *et al.*, 2002; Schaefer *et al.*, 2004; Costa *et al.* 2004) and X-ray diffraction (Cornu *et al.*, 1999; Sergio *et al.*, 2006). Liang *et al.* (2006) noted that ADEs are rich in kaolinitic clays that have reacted with a range of organic and other minerals. Liang *et al.* (2006) also found that the BC particles extracted from ADE consisted of highly aromatic, or only slightly oxidized organic carbon, which could not be found in organic matter extracts, bacteria or fungi. Novotny *et al.* (2007) found that different organic matter extracts from ADE have a higher content of aryl and ionisable oxygenated functional groups compared to adjacent soils. Moreover, observations by Liang *et al.* (2006) and Lehmann *et al.* (2005) in ADE, and Brodowski *et al.* (2006) in German chernozem have

Correspondence to: Paul Munroe, School of Material Science and Engineering, University of NSW, Sydney 2052, New South Wales, Australia. Tel: + 61 2 9385 4435; Fax: +61-2-9385-6400; e-mail: p.munroe@unsw.edu.au

shown that the BC particles are heterogeneous, which reflects their original diverse source materials (wood, leaves, crop residues, human and animal waste, shells and bones, fired pottery). The surfaces of ADE's are high in oxidized functional groups, which have originated either from oxidation of the BC itself or from adsorption of partially oxidized BC or non-BC materials (Lehmann *et al.*, 2005). Glaser *et al.* (2000) separated ADE into three different density fractions and SEM studies revealed BC particles intimately surrounded by mineral-rich phases. Solomon *et al.* (2007) concluded that the non-BC material in ADE could be the product of: (i) primary recalcitrant biomolecules from non-BC sources or (ii) secondary processes involving microbial-mediated oxidative or extracellular neoformation reactions of soil organic carbon from BC and non-BC sources, and stabilized through physical inaccessibility to decomposition agents because of sorption onto the surface or into porous structures of the BC particles, selective preservation or through intermolecular interactions involving clay, mineral nanoparticles and BC particles. Lehmann & Solomon (2010) note that the bonding between mineral matter and both BC and non-BC carbon is complex and cannot be resolved fully with methods such as NEXAFS.

Because high spatial resolution analysis has not been performed on these materials there is still considerable uncertainty as to the mechanisms of interactions between BC and mineral matter (Lehmann & Solomon, 2010). It is hypothesized that the formation of BC–mineral interactions occurs over multiple stages. First, the aluminosilicates and water (enriched in dissolved minerals and organic compounds) fill the pores of BC and react with the surfaces that have concentrations of acidic and basic functional groups, radicals, defects and mineral matter. These nanoscale mineral particles will react both chemically and electrochemically with the surfaces of BC to form organo-mineral complexes (Joseph *et al.*, 2010). Surface functional groups from BC or adsorbed soil organic matter may react with kaolinitic clays, which are common in highly weathered soils, through formation of hydrogen bonds and dipole interaction to silicate layers (Lagaly *et al.*, 1984). Complexation of silicic acid with phthalates may occur after dissolution of minerals such as silica by hydroxide ions that dissolve when BC is placed in the soil. Dead plant tissue and micro-organisms, which contain minerals, can be adsorbed onto the BC and clay surfaces (Amonette & Joseph, 2009). Micro-organisms existing in the very large macropores of BC can interact with minerals in complex ways (Gilbert & Banfield, 2005) and these composites can then react with the surfaces of the biochar. Larger BC pieces are broken into smaller particles over decadal time scales (Nguyen *et al.*, 2008) possibly via a range of different mechanisms resulting in higher surface area/volume ratios, which can then increase the rate of reaction with minerals and soil organic matter (Lehmann *et al.*, 2009). Over similar time scales, mineral elements such as Fe, Al and Si accumulate on ADE's surfaces, with still unidentified interactions (Nguyen *et al.*, 2008). However, it is not clear, how very old BC interacts on surface with mineral matter in soils.

Both, transmission electron microscopy (TEM) coupled with energy dispersive X-ray spectrometry (EDS) and scanning transmission electron microscopy (STEM) coupled with electron energy loss spectroscopy (EELS), provide detailed microstructural, crystallographic and microchemical analysis of materials at greater spatial resolution than methods such as SEM or NEXAFS. As soils are radiation sensitive materials, the resolution of the image will be dose-limited. Complementary analytical methods are therefore required. The 80–90% collection efficiency of EELS allows for the acquisition of much higher spatial resolution maps than it does for the ~1% collection efficiency for EDS. However, EDS can readily detect a much wider range of elements, especially at low concentrations, as the peak/background ratio is more favourable. These techniques have hitherto not been applied to ADE, principally because of the difficulty in making high-quality electron transparent specimens from such friable and heterogeneous materials. However, analysis through TEM-based methods provides an understanding of the distribution of different phases with high spatial resolution, together with information regarding the elemental chemistry and crystallography of the phases present (Williams & Carter, 2009). To our knowledge, this is the first study to report the structure of an ADE using complementary TEM-based analysis methods.

Therefore, this paper investigates the elemental composition of the BC–mineral interface at high spatial resolution, principally through the use of TEM and STEM. We hypothesize that certain elements preferentially accumulate which may provide indication for the types of interactions between mineral matter and BC surfaces.

Experimental procedure

Samples of microaggregate particles from two sites (Hatahara and Lago Grande) near Manaus, Brazil (3°8′S, 59°52′W), were examined. The physical and chemical properties have been analysed by Liang *et al.* (2006). The Anthrosols (locally known as 'Terra Preta de Indio') are the results of pre-Columbian settlements. Hatahara is of particular interest as it showed evidence of recent agricultural activities. A summary of the soils' properties are given in Table 1. The soil samples from each site were sieved to 2 mm before analysis.

Before TEM examination, the particles from each of these regions were examined using both a FEI Quanta 200 SEM (Hillsboro, OR, U.S.A.) and a Hitachi S3400 SEM (Mito City, Japan) fitted with an EDS detector. Approximately 20 particles were selected, mounted in epoxy resin and polished using standard metallographic techniques. Distinctive phases were identified and elemental analysis was performed using EDS. Emphasis of this examination was on the role of the heavier

Table 1. Summary of the chemical properties from BC-rich anthrosols from central Amazon (Liang *et al.*, 2006).

Site	Type	Depth (cm)	pH (1:2.5 H_2O)	Organic C (mg g^{-1})	Total N	C/N	Total P (mg kg^{-1})	Total Ca (mg kg^{-1})
Hatahara	Oxisol	43–69	6.4	22.0	1.0	23	9064	1 7545
Lago Grande	Oxisol	0–16	5.9	31.5	1.8	18	5026	6354

elements at the interface between carbon-rich and mineral-rich phases.

Thin electron transparent sections (100 nm thick and ~10 μm^2), suitable for TEM analysis, were then prepared at the boundary of a carbon-rich and an organo-clay phase using a FEI xP200 focused ion beam microscope (Hillsboro, OR, U.S.A.), using methods described elsewhere (Giannuzzi & Stevie, 1999). Sections were then examined using a Philips CM 200 TEM (Hillsboro, OR, U.S.A.) to which EDS facilities were attached. Typical sample preparation times were around 2 h. A further electron transparent section (<50 nm thick and 10 μm^2) was taken from a similar area using a FEI Strata 400 STEM focused ion beam (Hillsboro, OR, U.S.A.). This section was then examined using a NION UltraSTEM 100 (Kirkland, Washington, USA) fitted with an EELS detector. A further set of thinner specimens was prepared for STEM and EELS analysis to obtain high-quality images and spectra. The area around the region of interest was milled away using a 30 kV ion beam. A high current beam (6500 pA) was used to mill away the outer region and the beam current was slowly decreased from 6500 pA to a final current of 1000 pA as the specimen thickness approaches 1.5 μm. The specimen was then lifted out onto a TEM half grid using the FEI omniprobe *in situ* lift-out system. The specimen is then further milled until a thickness of ~200 nm with a final beam current of 70 pA. Finally, specimens were polished with a 5 kV ion beam, followed by a 2 kV ion beam, until a specimen thickness of ~50 nm was achieved. The low-energy mills were used to remove any unwanted damage created by the higher voltage ion beam. Given the heterogeneous nature of ADE, TEM and STEM examination of the cross section of ADE was performed for over 20 different regions across several TEM sections. The TEM data shown is representative of these different regions.

Results and discussion

SEM analysis

A low magnification backscattered electron image (Fig. 1a) reveals the extreme heterogeneity of the ADE specimen. A higher magnification backscattered electron image (Fig. 1b) depicts a representative BC particle embedded within a matrix of microaggregated mineral matter. EDS analysis shows that (Fig. 1c) the mineral matrix is largely composed of aluminosilicate and that the BC particle (Fig. 1d) is enriched in calcium and chlorine. (The chromium peak observed around 5.5 keV arises from the conductive chromium coating applied before analysis.) None of these C-enriched regions exhibited any of the characteristic macroporous structures of wood-derived biochars (Chia *et al.*, 2010). This observation is similar to that of Glaser *et al.* (2000) who found in the heavy density fraction of ADE, a BC particle embedded in a cluster of iron and aluminium-rich oxides. A micrometre-scale thick darkly imaging shell at the BC–mineral interface is characteristic, as evident from similar particles in Figure 1(a). This darker contrast is indicative of a depletion of calcium within the BC at the interface (Fig. 1e). This observation differs from that of Liang *et al.* (2006), where a great proportion of cations (in relation to carbon) were found near the edges of the BC particle.

Within the microaggregates there are regions (labelled C in Fig. 2a) of high Si and O content [presumably silica based (Fig. 2c)]. Particles that appeared similar to the silica particles were also detected (labelled D in Fig. 2a). However, the EDS spectrum shown in Figure 2(d) shows that these particles are enriched in Al, Si, Na and O (and are presumably clay particles). Sub-micrometre regions, which exhibit distinctive circular structures, were also found embedded in the aluminosilicate matrix that have high calcium or silica content that could possibly be the remnants of diatoms or micro-organisms in some of the porous areas within the microaggregates (Ransom *et al.*, 1997; Ransom *et al.*, 1999).

Figure 3 shows a series of elemental maps recorded using EDS from a polished section of the ADE. This illustrates the heterogeneity of the aggregates both in terms of the distribution of phases/particles and elements within these regions. A particle enriched in Ca and C (labelled A) is located next to a particle enriched in Al, Si and O (labelled B). There are two particles labelled C and D, respectively, that each has significant calcium and phosphorous concentrations, presumably calcium phosphate particles. Each of these four particles are surrounded by a region that has a variable composition of elements such as Al, Si, O, C, Ca, P and Fe. Ca- and P-enriched regions were distributed randomly within the matrix around this carbon-enriched particle. There are a considerable number of sub-micrometre titanium oxide particles distributed throughout this area, as seen in the Ti map.

TEM analysis

Figure 4 shows bright field TEM images of the microstructure of ADE. In this case the thin section was prepared from the region indicated by the line shown in Figure 1(b). Figure 4(a)

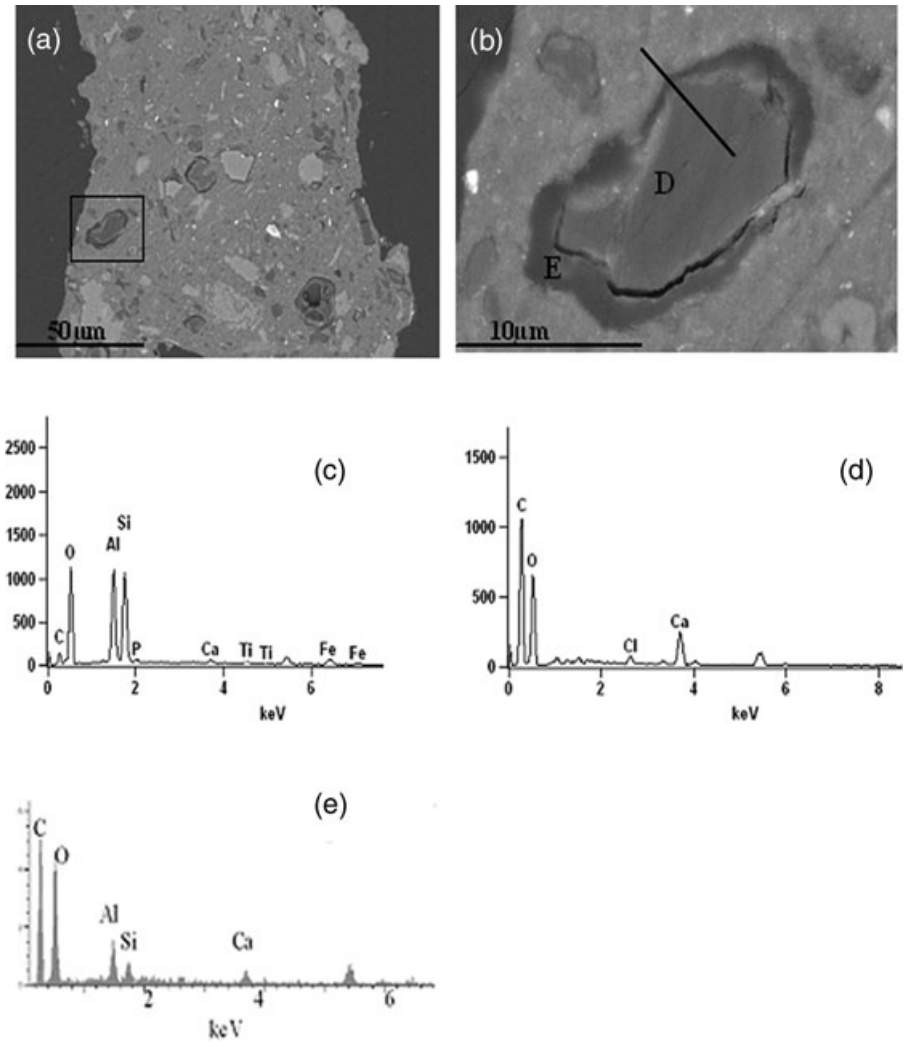

Fig. 1. SEM data acquired from a typical ADE soil specimen: (a, b) backscattered electron images and (c, d) representative EDS spectra. Panel (a) is a low magnification image. A high magnification image of the carbon-enriched region is shown in (b). EDS spectrum of the mineral matrix (labelled C in a) is shown in (c). An EDS spectrum of the black carbon particle (labelled D) shows it is enriched in calcium and chlorine is shown in (d). An EDS spectrum from the shell exhibiting darker contrast area surrounding the black carbon particle is shown in (e). A line has been added to (b) to show the location of the TEM specimen discussed in Figure 4.

shows a carbon-enriched area (marked C) surrounded by an aggregate of organo-clay regions which are enriched in Al, Si and Fe. The carbon-enriched region presumably originates from BC, because of its high Ca content and low O/C ratio (EDS data is shown in Fig. 4c), which is consistent with the EDS data shown in Figure 1(d). This phase was shown by electron diffraction to be amorphous that is simple ring patterns (not shown here) were obtained from these regions. The presence of calcium in carbon may be covalently bonded with functional groups within the lattice, or ionically bonded with the carbon lattice, as well as being a constituent of any polysaccharides that may form a complex with the clay nanoparticles (darker areas; Joseph *et al.*, 2010). A higher magnification image of the interface between the organo-clay region and the carbon-enriched phase is shown in Figure 4(b). The clay particles that are enriched in Al, Si and O content are shown to exist either as nanotubes around 10–50 nm in length or as aggregates of platelets around 20 nm in diameter. The darker particles labelled D in Figure 4(b), which are enriched in Ca and/or Fe and O, are found embedded throughout the carbon matrix as well. Pores less than 100 nm in diameter are also found in this interface region.

Figure 5 shows a series of elemental X-ray maps recorded from an ADE particle. These reveal the distribution of mineral particles around an amorphous carbon-enriched region (labelled A). The high Al/Si/O content suggests that the region labelled B is clay consisting of platelets ∼50–100 nm in length. Some of these platelets are porous and have a tubular morphology that could signify that they are delaminated kaolinite formed via intercalation (Matusik *et al.*,

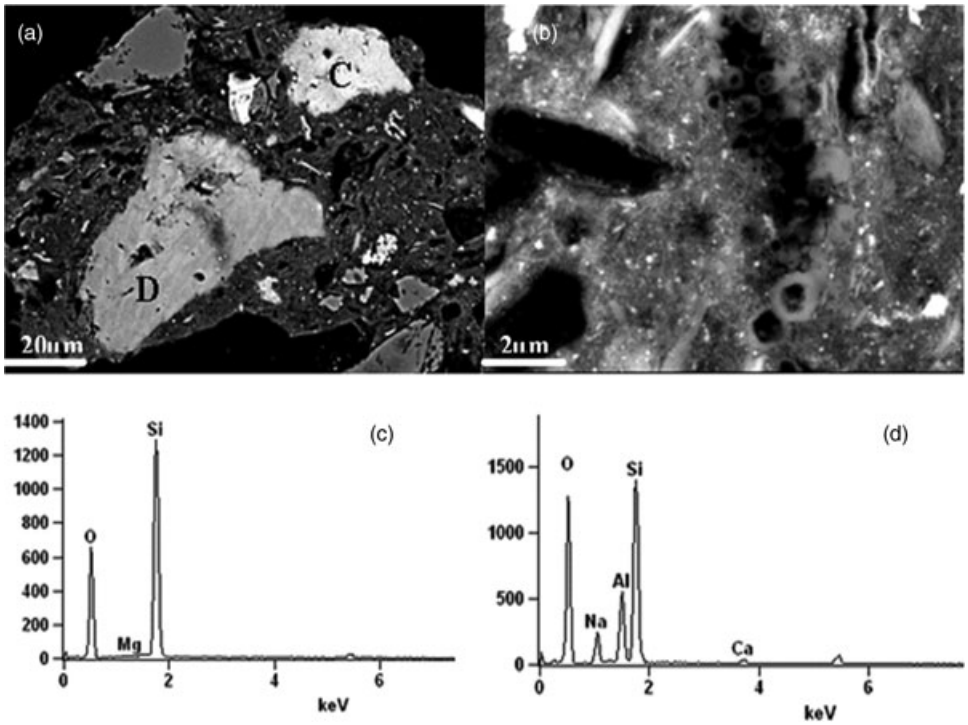

Fig. 2. SEM data acquired from polished ADE sections: (a, b) backscattered electron images and (c, d) representative EDS spectra. Panel (a) shows an ADE aggregate with two distinct regions which are labelled C and D. Particle C is presumably a silica particle, whereas particle D is presumably a clay particle. The corresponding EDS spectra are shown in (c) and (d). Sub-micrometre pores which were found on the aluminosilicates matrix are shown in (b).

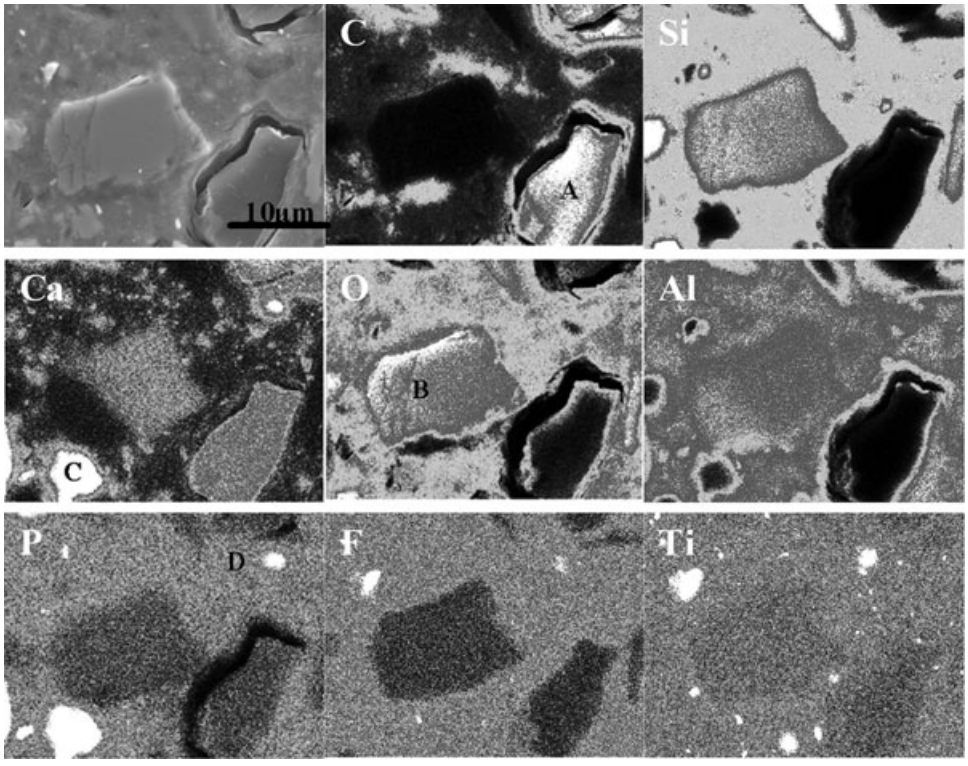

Fig. 3. EDS elemental maps of the internal structure of an ADE particle. Four regions with different chemical compositions were identified in the analysed area. Region A is enriched in C and Ca, region B is enriched in Si and O, region C and D is enriched in Ca and P and there are also regions that are enriched in Ti distributed throughout the matrix as seen in the Ti map.

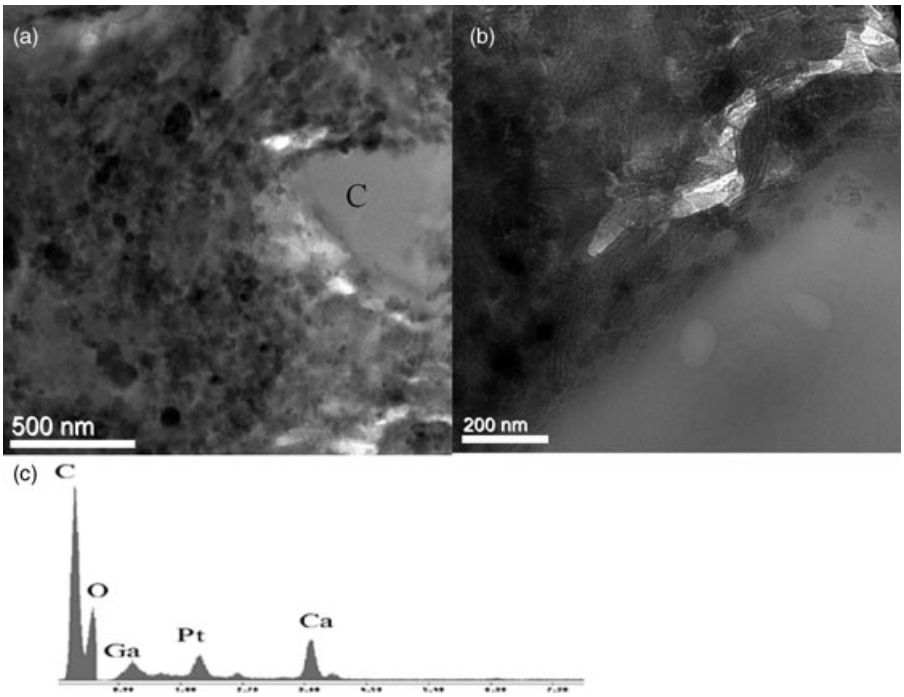

Fig. 4. A bright field TEM image (a) of an ADE particle. Panel (b) shows a bright field TEM image of the interface between the mineral-rich phase and amorphous carbon with a high calcium content. The corresponding EDS spectrum of the calcium-enriched carbon phase is shown in (c).

2009). TEM studies by Joussein (2005) indicate structures similar to those shown in Figure 4. Similarly, Churchman *et al.* (1995) found small tubes (<80 nm in diameter) that included central cylindrical pores of between 5 nm and 15 nm in diameter, whilst the centres of large tubes (>1 μm in width) were largely filled, so that they included virtually no cylindrical pores. It can also be seen that there appears to be a thin layer of Mn-rich nanoparticles, presumably oxides, which lie at the interface between the BC and the clay-based region. These particles, themselves, are embedded in a carbon-enriched region. There is also a random distribution of iron oxide microparticles within the clay phase.

Figure 6 illustrates the complex nature of the sub-micrometre microaggregate. A BC particle evident in this map shows an elemental distribution consistent with that in Figure 1, with calcium enrichment within much of the particle, but a calcium-depleted (and carbon-enriched) zone at the interface with adjacent mineral phases. K is associated both

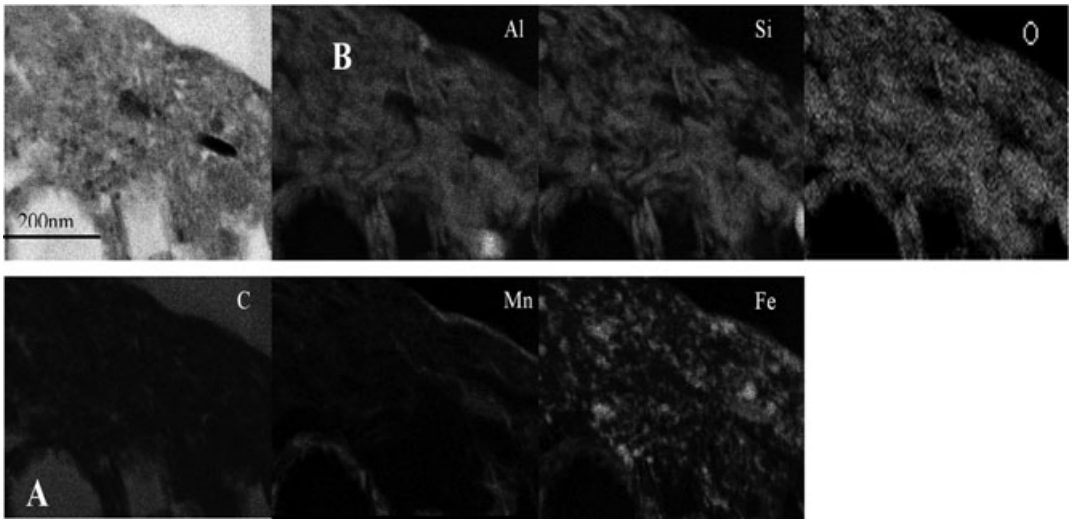

Fig. 5. Elemental EDS maps showing a mineral aggregate (labelled B) surrounding a carbon-enriched particle (labelled A). Iron oxides particles are found distributed randomly across the aggregate.

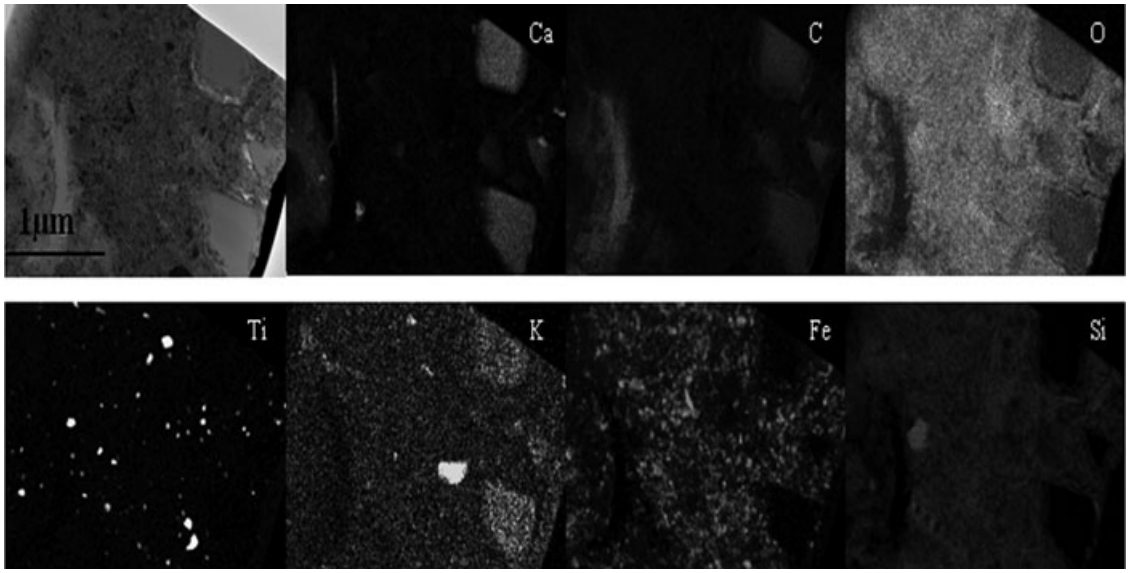

Fig. 6. Elemental EDS maps showing a calcium-enriched carbon embedded in a mineral-rich matrix. Iron oxides and titanium oxides particles are found distributed randomly across the matrix.

with the carbon-enriched particles as well existing as a salt (possibly KCl). Silicon and magnesium exist as both an oxide particles as well as a component in the clay. Iron oxide and titanium oxide microparticles are scattered randomly within the clay phase, which is similar to what was found in Figure 5.

STEM analysis

An electron transparent thin section was prepared from a region across the interface between a carbon-enriched region and a mineral-enriched region, similar to the area shown in Figure 1(b) and examined by STEM. This analysis showed that the interfaces between the organic and mineral regions are both heterogeneous and complex. EELS analysis was used, in conjunction with STEM, as it is better suited to resolve the internal structure of nanoparticles and surface segregants for the major constituent elements compared to EDS. For instance, low concentrations of Mg and K were easier to detect by EDS than EELS.

Figures 7(a)–(d) show two areas adjacent to the interface between the BC and the mineral region. The mineral matrix comprises clusters of iron oxide particles that are less than 10 nm in diameter that have both precipitated on the clay particles and between the clay particles. Much larger TiO_2 particles are coated with both clay and iron oxide particles. A carbon-enriched phase binds all of these minerals together. Figure 6(e) shows a larger iron-based particle that has been identified using lattice fringes (not shown) as goethite.

Figure 8 depicts a series of EELS maps of the region of interest, where a brighter contrast means a higher concentration of that particular element in that region. The EELS maps shown in Figure 8 are generic representation of a typical ADE particle. Figure 8(a) shows an annular dark field STEM image of ADE in which the field of view is adjacent to the area shown in Figure 7. The EELS maps are taken from the boxed region shown in Figure 8(a), where at the clay–organic interface shows the infiltration of carbon and iron (arrows) around the clay particles. Figure (b) is the C-K edge, (c) the Ca $L_{2,3}$ edge, (d) the O-K edge from an energy range of 535–540 eV, where the signal from aluminosilicate (Fig. 8f) dominates over the Fe-oxide bonding and (e) Fe $L_{2,3}$ edge. Figure 8(f) shows EELS spectra from both aluminosilicate and iron hydroxide regions, which shows the contrasting oxygen signals from these two phases. There are a number of interesting features that help elucidate the bonding mechanisms. Firstly, areas of the organic layer between the two particles may comprise a compound (or compounds) that is less than 10–20 atoms thick. Some of these compounds have a high Ca content and these predominate around the clay particle.

The STEM and TEM examination of these particles has highlighted the role of Fe and, to a lesser extent, Mn, at the interfaces between the amorphous carbon and clay particles. It is apparent from both EDS and EELS analysis that the Fe may be part of the kaolinitic clay lattice structure, which exists either as crystalline nanoparticles or in the form of an amorphous precipitate phase. Gilbert & Banfield (2005) note that nanoparticles (especially Fe and Mn oxides) can either precipitate on, or the ions can adsorb on, the surfaces of micro-organisms forming amorphous phases. Organic macromolecules secreted by microbes can react with ions

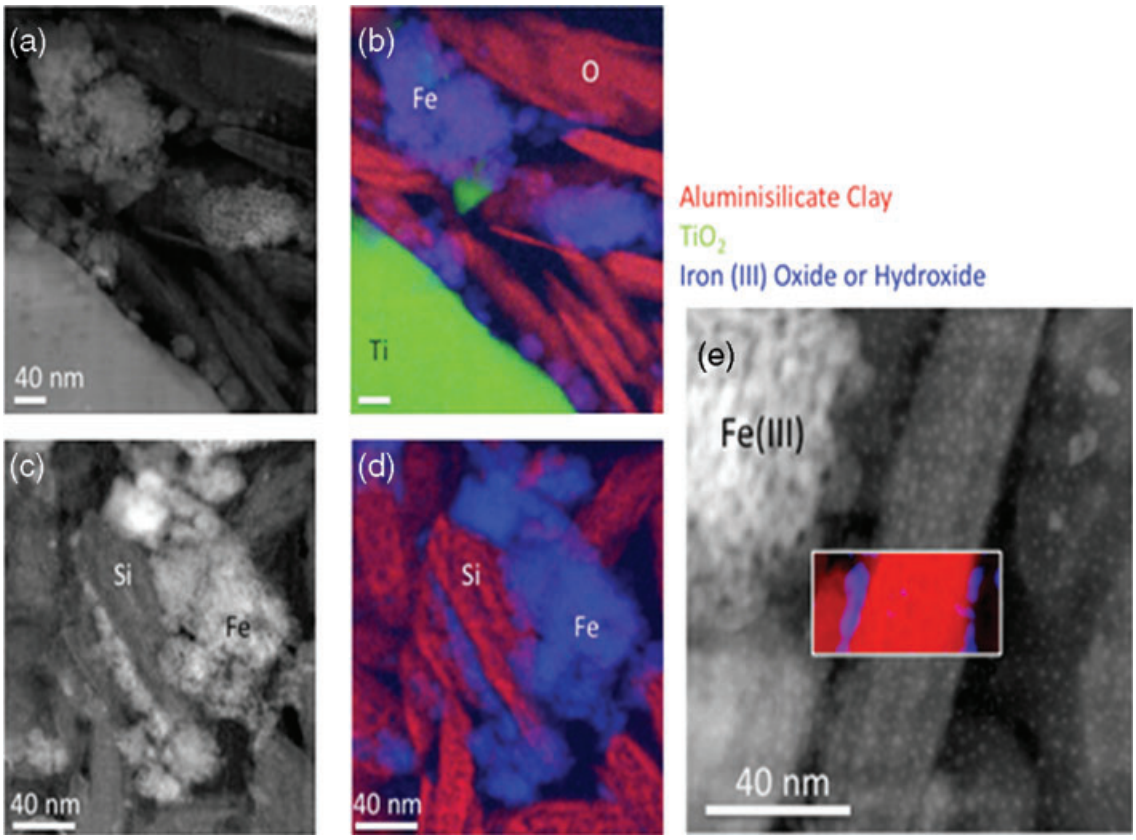

Fig. 7. Dark field (a, c) STEM images and their respective EELS map (b, d) showing the heterogeneous nature of an ADE particle. The iron-enriched particle shown in (e) is goethite.

or compounds in the environment, resulting in deposition of mineral particles. The strong negative charge on the microbial cell walls also provides multiple sites for metal binding. The cations from the environment will be attracted by the negatively charged carboxyl groups on the cell walls and these will promote the nucleation for biomineral crystal growth. (Gilbert *et al.*, 2005)

There is considerable nanoscale porosity at the interface between the carbon-based region and the various mineral phases. It is also apparent that TiO_x and SiO_x nanoparticles are possibly bonded to the carbon-based region, the clay and the iron-enriched phase. This indicates that redox reactions play an important part in the formation of these organo-mineral aggregates. Tropical soils are subjected to large rain events that can cause changes in pH of 1–2 units within a few days resulting in changes in the equilibrium between Fe^{2+} and Fe^{3+} ions (Thompson *et al.*, 2006). Thompson *et al.* (2006) have noted that changes in pH can cause either colloidal dispersion (high pH) or coagulation (low pH) or neoformation of colloidal Fe-oxides and/or Fe^{3+} natural organic metal complexes. These reactions are further complicated because of catalysis of the reduction portion of the Fe redox cycle by micro-organisms. Redox reactions of minerals and ions in solution, as well as other inorganic molecules, provide metabolic energy for prokaryotes. (Gilbert *et al.*, 2005) They also noted that the concentration of electron donors (e.g. organic C) and acceptors (e.g. O_2, NO_3^-, etc.) and microbial population dynamics potentially influence colloidal stability in soils via biogeochemical pathways.

Thompson *et al.* (2009) subjected soil from Maui, Hawaii to a series of wetting and drying cycles to alter both pH and Eh. They found mobilization of refractory Ti, as well as Si and Al, with changes in pH. TEM examination of the colloids revealed structures containing mineral particles with diameters of 1–5 nm that were held together by a material rich in organic carbon (that also noted adsorbed metal ions). Some colloid particles were crystalline, whereas others were composed of Fe, Al and Si, with variable Ti concentration. These structures were similar to those observed in the ADE examined in this paper.

As Kirk (2004) has pointed out, reduction of submerged soils proceeds roughly in the sequence predicted by thermodynamics and this might explain the high Mn content around some BC particles. Thus, it is possible that the sequence of stabilizations reactions involves an initial oxidation of the carbon both from the BC and from soil organic matter and then

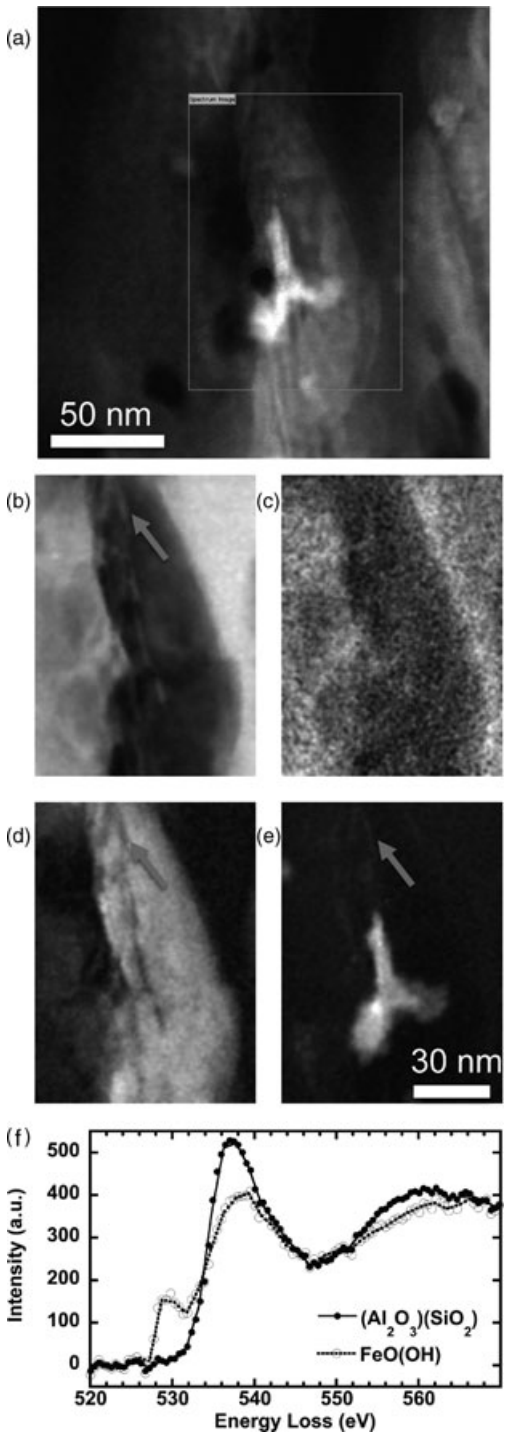

Fig. 8. (a) Annular dark field STEM image showing a wider view of the area where the EELS maps were recorded. Panels (b)–(e) depict EELS maps at the clay–organic interface showing the infiltration of carbon and iron around the clay particles. (b) C-K edge. (c) Ca $L_{2,3}$ edge (d) O-K edge from 535 eV to 540 eV where the signal from aluminosilicates dominates over Fe-oxide bonding and (e) Fe $L_{2,3}$ edge. Figure 8(f) shows EELS spectra over an energy range from 520 eV to 570 eV, for aluminosilicates and iron hydroxide.

during the rain events a reduction of the MnO_2 at the surface to form cations, which then bond with the negatively charged carbon surfaces of the BC or non-BC. Bonding may take a number of forms depending on the specific surface functional groups on the carbon. Violante & Gianfreda (2000) and Joseph *et al.* (2010) note that the bonding that takes place could be a result of acid–base reactions with surface COOH, C-OH, C=O, C-O and CN functional groups, coordination of deprotonated OH or COOH functional groups, ligand exchange, coordination of dissolved multidentate ligand with both metal ions of the surface of the biochar and the dissolved metals ions, and Cπ–cation interactions. It is also possible that the formation of some of the pores at the BC–mineral interfaces is because of the formation of gaseous CO_2

Mineral phases present in rocks that are exposed to water and air liberate ions that can reprecipitate to form nanoparticles, such as oxides, phosphates and clay minerals. (Gilbert & Banfield, 2005) Iron oxyhydroxides are accumulated through the oxidation of iron in acidic and near-neutral solutions by micro-organisms (Banfield *et al.,* 2000). Mineral transformations of the precipitated hydrous ferric oxides can produce nanocrystalline iron oxides, such as goethite or hematite. (Benner *et al.*, 2002; Hansel *et al.*, 2003) Crystal growth is accomplished by eliminating water molecules at interfaces and forming iron–oxygen bonds. This would account for the observations of the coexistence of amorphous and crystalline Fe seen in the BC STEM images (data not shown). This may influence metabolic activity or micro-organisms by restricting communication between a cell and its surroundings. It may also provide beneficial effects through protection from predators, inhibit desiccation and screen cells from ultraviolet radiation.

Kaolinite is known to react with acetates (Lagaly *et al.*, 2006) and organic compounds with nitrogen and sulphur functional groups to form tube- or rod-like structures (Nakagaki *et al.*, 2006). The compounds initially penetrate the silicate layers with the result that one or two of the layers start to curl. Lagaly *et al.* (2006) note that even weak mechanical forces can then cause the kaolinite to delaminate and form tube-like structures. Alternately, the Al/Si/O particles with tube-like structures could be allophanes (Gustafsson *et al.*, 1999; Joussein *et al.*, 2005). These are possibly formed because of the reaction and coprecipitation of Al species and silicic acid when the pH is between 5 and 7 (Parfitt, 2009). The specific mechanisms for formation are still not clear (Joussein *et al.*, 2005) and would require further studies. Parfitt (2009) note that these tubular structures could play a role in the stabilization of soil organic matter, increased cation exchange capacity and especially because of the water capacity of Terra Preta soils. Similar dark earths have been found in regions other than the Amazon, for example the European plaggen soils and more recently, anthropogenic soils in Australia (Downie *et al.*, 2011). These soils have not been studied using

high-resolution methods, such as those employed here, but it is possible that the interactions observed in this study might also occur in these soils.

Conclusions

Organo-clay microaggregates formed in ADE are structurally very complex. There are a number of features in common that have been observed for a majority of particles examined, namely:

1. There is a C/O-enriched region that has a very high concentration of amorphous carbon that also can have a significant Ca concentration.
2. Most of the carbon-enriched regions examined, exist at the edge of the microaggregate and are surrounded by a region composed of clay nanopartricles bonded together with an amorphous carbon that contains a significant calcium content. There is a high density of micropores at this interface.
3. The bonding between the organo-clay regions and the amorphous carbon phase and between the clay nanoparticles and the amorphous carbon phase is complex and probably involves biotic and/or abiotic processes.
4. Distribution of other mineral particles within the microaggregate appears to be random which would suggest that the aggregates form over a considerable period of time. Different mechanisms are likely associated with the agglomeration of these different regions.
5. The nanoparticles that were distributed randomly across the sample can be a product of biotic (aggregated together by the negatively charged carboxyl groups found in the cell wall) or abiotic process (precipitation of ions from solution).
6. Cracks within the silica particles also appear to be the repository of organo-clay complexes.
7. The interfaces between the different phases within the microaggregates are heterogeneous and are complex.

References

Amonette, J.E. & Joseph, S. (2009) Physical properties of biochar. Biochar for environmental management. *Science and Technology*. (ed. by J. Lehmann and S Joseph), pp. 33–53. Earthscan, London.

Benner, S.G., Hansel, C.M., Wielinga, B.W., Barber, T.M. & Fendorf, S. (2002) Reductive dissolution and biomineralization of iron hydroxide under dynamic flow conditions. *Environ Sci Technol.* **36**, 1705–1711.

Brodowski, S., Amelung, W., Haumeier, L., Abetz, C. & Zech, W. (2005) Morphological and chemical properties of black carbon in physical soil fractions as revealed by scanning electron microscopy and energy-dispersive X-ray spectroscopy. *Geoderma* **128**, 116–129.

Brodowski, S., John, B., Flessa, H. & Amelung, W. (2006) Aggregate-occluded black carbon in soil. *Eur J. Soil Sci.* **57**, 539–546.

Chia, C.H., Munroe, P., Joseph, S. & Lin, Y. (2010) Microscopic characterisation of synthetic Terra Preta. *Australian J. Soil Res.* **48**, 593–605.

Churchman, G.J., Davy, T.J., Aylmore, L.A.G., Gilkes, R.J. & Self, P.G. (1995) Characteristics of fine pores in some halloysites. *Clay Minerals* **30**, 89–98.

Cornu, S., Lucas, Y., Lebon, E., Ambrosi, J.P., Luizao, F., Rouiller, J., Bonnay, M. & Neal, C. (1999) Evidence of titanium mobility in soil profiles, Manaus, Central Amazonia. *Geoderma* **91**, 281–295.

Downie, A.E., Van Zwieten, L., Smernik, R. & Munroe, P. (2011) Discovering Terra Preta Australis: rethinking temperate soils capacity to sequester carbon. *Agric, Ecosystems and Environ* **140**, 137–147.

Glaser, B., Balashov, E., Haumaier, L., Guggenberger, G. and Zech, W. (2000) Black carbon in density fractions of anthropogenic soils of the Brazilian Amazon region. *Organic Geochem* **31**, 669–678.

Giannuzzi, L.A. & Stevie, F.A. (1999) A review of focused ion beam milling techniques for TEM specimen preparation. *Micron* **30**, 197–204.

Gilbert, B. & Banfield, J.F. (2005) Molecular-scale processes involving nanoparticulate minerals in biogeochemical systems. *Rev Mineral Geochem* **59**, 109–155.

Gilbert, P.U.P.A., Abrecht, M. & Frazer, B.H. (2005) The Organic-Mineral Interface in Biominerals. *Rev Mineral Geochem* **59**, 157–185.

Gustafsson, J.P., Bhattacharya, P. & Karltun, E. (1999) Mineralogy of poorly crystalline aluminium phases in the B horizon of Podzols in southern Sweden. *Appl. Geochem.* **14**, 707–718.

Hansel, C.M., Benner, S.G., Neiss, J., Dohnalkova, A., Kukkadapu, R.K. & Fendorf, S. (2003) Secondary mineralization pathways induced by dissimilatory iron reduction of ferrihydrite under advective flow. *Geochim. Cosmochim. Acta* **67**, 2977–2992.

Joseph, S.D., Camps-Arbestain, M., Lin, Y., *et al.* (2010) An investigation into the reactions of biochar in soil. *Australian J. Soil Res.* **48**, 501–515.

Joussein, E., Petit, S., Churchman, J., Theng, B., Righi, D. & Delvaux, B. (2005) Halloysite clay minerals – A review. *Clay Miner.* **40**, 383–426.

Kirk, G. (2004) Reduction and oxidation. *The Biogeochemistry of Submerged Soils*, pp. 92–134. John Wiley & Sons, Chichester.

Lagaly, G., Barrer, R.M. & Goulding, K. (1984) Clay minerals: their structure, behaviour and use, philosophical transactions of the Royal Society of London. *Series A, Math. Phys Sci* **311**, 315–332.

Lagaly, G., Ogawa, M. and Dékány, I. (2006) Clay Mineral Organic Interactions. In: *Handbook of Clay Science* vol. 1. (ed. by F. Bergaya, B.K.G. Theng & G. Lagaly), pp. 309–377. Elsevier, Amsterdam.

Lehmann, J. & Solomon, D. (2010) Organic carbon chemistry in soils observed by synchrotron-based spectroscopy. *Synchroton-based Techniques in Soils and Sediment*. (ed. by B. Singh and M. Gräfe), pp. 289–312. Elsevier, Amsterdam.

Lehmann, J., Liang, B., Solomon, D., Lerotic, M., *et al.* (2005) Near-edge X-ray absorption fine structure (NEXAFS) spectroscopy for mapping nano-scale distribution of organic carbon forms in soil: application to black carbon particles. *Global Biogeochem Cycles* **19**: GB1013. DOI 10.1029/2004GB002435.

Lehmann, J., Kinyangi, J. & Solomon, D. (2007) Organic matter stabilization in soil microaggregates: implications from spatial heterogeneity of organic carbon contents and carbon forms. *Biogeochem.* **85**, 45–57.

Lehmann, J., Solomon, D., Kinyangi, J., Dathe, L., Wirick, S. & Jacobsen, C. (2008) Spatial complexity of soil organic matter forms at nanometre scales. *Nature Geoscience* **1**, 238–242.

Liang, B., Lehmann, J., Solomon, D., *et al* (2006) Black carbon increases cation exchange capacity in soils. *Soil Sci Soc Am. J.* **70**, 1719–1730.

Lima, H.N., Schaefer, C.E.R., Mello, J.W.V., Gilkes, R.J. & Ker, J.C. (2002) Pedogenesis and pre-Colombian land use of "Terra Preta Anthrosols"

("Indian black earth") of western Amazonia. *Geoderma* **110**, 1–17.

Matusik, J., Gawel, A., Bielanska, E., Osuch, W. & Bahranowski, K. (2009) The effect if structural order on nanotubes derived from kaolin-group minerals. *Clay Clay Miner.* **47**, 452–464.

Nakagaki, S., Machado, G.S., Matilte, H.M., Marangon, A.A., di Castro, K.A., Ney, M.N. & Wypych, F. (2006) Immobilization of iron porphyrins in tubular kaolinite obtained by an intercalation/delamination procedure. *J Catalysis*. **242**, 110–117.

Nguyen, B., Lehmann, J., Kinyangi, J., Smernik, R., Riha, S.J. & Engelhard, M.H. (2008) Long-term black carbon dynamics in cultivated soil. *Biogeochemistry* **89**, 295–308.

Novotny, E.H., Hayes, M.H.B., deAzevedo, E.R. & Bonagamba, T.J. (2006) Characterisation of Black Carbon rich samples by 13C solid-state nuclear magnetic resonance. *Naturwissenschaften* **93**, 447–450.

Novotny, E.H., deAzevedo, E.R., Bonagamba, T.J., Cunha, T.J.F., Madari, B.E., Benites, V.dM., Hayes, M.H.B. (2007) Studies of the compositions of humic acids from Amazonian dark darth soils, *Environ. Sci. Technol.* **41**, 400–405.

Novotny, E.H., Hayes, M.H.B., Madari, B.E., *et al.* (2009) Lessons from the Terra Preta de Índios of the Amazon region for the utilisation of charcoal for soil amendment, *J. Braz. Chem. Soc.* **20**, 1003–1010.

Parfitt, R.L. (2009) Allophane and imogolite: role in soil biogeochical processes. *Clay Miner.* **44**, 135–155.

Ransom, B., Bennett, R.H., Baerwald, R. & Shea, K. (1997) TEM study of in situ organic matter on continental margins: occurrence and the "monolayer" hypothesis. *Mar. Geol.* **138**, 1–9.

Ransom, B., Bennett, R.H., Baerwald, R., Hulbert, M. & Burkett, P. (1999) In situ conditions and interactions between microbes and minerals in fine-grained marine sediments: a TEM microfabric perspective. *Am. Mineral.* **84**, 183–192.

Schaefer, C.E.G.R., Lima, H.N., Gilkes, R.J. & Mello, J.W.V. (2004) Micromorphology and electron microprobe analysis of phosphorous and potassium forms of indian black earth (IBE) anthrosol from Western Amazonia. *Aust. J. Soil Res.* **42**, 401–409.

Schmidt, M.W.I. & Noack, A.G. (2000) Black carbon in soils and sediments: analysis, distribution, implications, and current challenges. *Global Biogeochem. Cycl.* **14**, 777–793.

Sergio, C.S., Santana, G.P., da Costa, G.M. & Horbe, A.M.C. (2006) Identification and characterization of maghemite in ceramic artefacts and archaeological black earth of Amazon region. *Soil Sci* **171**, 59–64.

Six, J., Elliott, E.T., Paustian, K. & Doran, J.W. (1998) Aggregation and soil organic matter accumulation in cultivated and native grassland soils. *Soil Sci. Soc. Am. J.* **62**, 1367–1377.

Six, J., Guggenberger, G., Paustian, K., Haumaier, L., Elliott, E.T. & Zech, W. (2001) Sources and composition of soil organic matter fractions between and within aggregates. *Eur. J. Soil Sci.* **52**, 607–618.

Solomon, D., Lehmann, J., Thies, J., *et al.* (2007) Molecular signature and sources of biochemical recalcitrance of organic C in Amazonian dark earths. *Geochim. Cosmochim. Acta* **71**, 2285–2298.

Thompson, A., Rancourt, D., Chadwick, O. & Chorover, J.D. (2009) Influence of redox fluctuations and rainfall on pedogenic iron alteration and soil magnetic properties. *Proceedings of the American Geophysical Union, Fall Meeting 2009*, abstract #GP41C-05

Violante, A. & Gianfreda, L. (2000) The role of biomolecules in the formation and reactivity towards nutrient and organics of variable charge minerals and organominerals. *Soil Biochemistry* (ed. by J. Bollag & G. Stotzky) Marcel Dekker, New York, pp. 207–270.

Williams, D.B. & Carter, C.B. (2009) *Transmission Electron Microscopy: a Textbook for Materials Science*, 2nd edn. Springer, New York.